

# Target switching in curved human arm movements is predicted by changing a single control parameter

Heiko Hoffmann

Received: 24 September 2009 / Accepted: 10 October 2010

**Abstract** Straight-line movements have been studied extensively in the human motor-control literature, but little is known about how to generate curved movements and how to adjust them in a dynamic environment. The present work studied, for the first time to my knowledge, how humans adjust curved hand movements to a target that switches location. Subjects ( $n=8$ ) sat in front of a drawing tablet and looked at a screen. They moved a cursor on a curved trajectory (spiral or oval shaped) towards a goal point. In half of the trials, this goal switched 200 ms after movement onset to either one of two alternative positions, and subjects smoothly adjusted their movements to the new goal. To explain this adjustment, we compared three computational models: a superposition of curved and minimum-jerk movements (Flash and Henis, 1991), Vector Planning (Gordon et al, 1994) adapted to curved movements (Rescale), and a non-linear dynamical system, which could generate arbitrarily-curved smooth movements and had a point attractor at the goal. For each model, we predicted the trajectory adjustment to the target switch by changing only the goal position in the model. As result, the dynamical model could explain the observed switch behavior significantly better than the two alternative models (spiral:  $p = 0.0002$  vs Flash,  $p = 0.002$  vs Rescale; oval:  $p = 0.04$  vs Flash;  $p$  values obtained from Wilcoxon test on  $R^2$  values). We conclude that generalizing arbitrary hand trajectories to new targets may be explained by switching a single control command, without the need to re-plan or re-optimize the whole movement or superimpose movements.

**Keywords** Behavioral experiment · Target switch · Curved movement · Computational model · Dynamical system · Convergent force field

## 1 Introduction

Humans can move a hand smoothly in a straight or curved path towards a target and adjust in mid-flight if the target moves. Despite the apparent ease of this task, little is known about how humans generate curved movements and adjust them to a changing environment. Likewise, generating artificially human-like motion remains a challenge, whose solution would benefit the control of prosthetic and electrically-stimulated paralyzed limbs.

One approach to generate a movement trajectory is through optimization. This approach, as a model of human motor control, has been popular for some decades (Flash and Hogan, 1985; Stein et al, 1986; Kawato, 1996; Harris and Wolpert, 1998; Todorov and Jordan, 1998). Optimal or near optimal movements may be obtained at a planning stage given a certain cost, e.g., minimum jerk, minimum torque change, or minimum task variance. This optimization, however, does not account for target changes during a movement. For a new target, the movement has to be re-optimized, but such a step may be computationally too costly to allow a quick adjustment in a dynamic environment.

Alternatively, we can describe a movement as being generated by a dynamical-system equation. For example, “next-state planning” models (Bullock and Grossberg, 1988; Shadmehr and Wise, 2005) do not assume a precomputed trajectory, but update the state of the moving limb given the current state and goal of the movement. Next-state planners can be formulated as

differential equations. For instance, Hoff and Arbib (1993) reformulated the minimum jerk approach as differential equation, where a change in goal state immediately adjusts the movement trajectory towards the new target. This model, however, is restricted to point-to-point movements, and thus cannot describe the adjustment of curved movements - unless the model would be embedded in a complex via-point planner (Viviani and Flash, 1995).

In laboratories, most studied movements are indeed point-to-point or straight. However, humans perform a wide variety of curved movements in daily life. To acknowledge this fact, we study in this article curved movements, particularly, their adjustment to new targets.

We introduce a computational model that can generate straight and curved movements. From the model's perspective there is no fundamental difference between the two. In a related model, Ijspeert et al (2002, 2003) extended the next-state planner to arbitrary trajectories, as discussed in Shadmehr and Wise (2005). Similar to Bullock and Grossberg (1988), they worked with differential equations, but could apply learning mechanisms, such that these equations could reproduce any desired trajectory, while guaranteeing that the movement converges at the goal point. In its original form, however, these equations cannot predict human-like adjustment of movements (Hoffmann et al, 2009). Here, using also the concept of dynamical systems, we provide new equations that overcome this limitation.

In a behavioral experiment, we study how humans spontaneously change curved movements to end at a new target. To model this change, we build a computational model based on dynamical systems. Starting from the dynamics equation of the human arm and its hypothesized controller, we make numerically-justified approximations to arrive at a simplified model equation. In this work, we try to keep the model as simple as possible to avoid the lack of explanatory power associated with complex models, where, e.g., parameters could be tuned to fit any data (Alexander, 1995).

Our model has two key features: first, it can be adapted to generate any arbitrary smooth limb movement, particularly, the curved movements used in our experiments. Second, towards the end of a movement, the dynamics are governed by a point-attractor, which guarantees convergence to the goal position. This model is at the heart of current research in human motor control: psychophysical evidence suggests that trajectory control and end-point positional control are two independent control processes that are combined through a smooth transition (Ghez et al, 2007; Scheidt and Ghez, 2007).

As result of our model equations, trajectories adjust to new target positions by changing solely the position of this goal-point attractor. We test if switching this position during a movement explains the experimentally-observed change in movement trajectories resulting from the target switch.

We compare our model with two alternatives: first, a superposition of a curved and a straight, minimum-jerk movement (Flash and Henis, 1991) and, second, an adaptation of the Vectorial Planning hypothesis (Gordon et al, 1994; Krakauer et al, 2000). Both have been suggested to simplify planning and movement generation through reduction of control parameters. We adapt both models to reproduce the observed curved movements in our experiment (when no goal switch occurred) and to predict a movement adjustment to a new goal position, just as a result of changing this position in the model. We chose these models due to their simplicity: our adaptation is straight forward, no parameter tuning is necessary, and the goal position alone determines the movement adjustment.

The first alternative model (*Flash*) is based upon work that shows that human reaching trajectories resemble those that minimize jerk (Flash and Hogan, 1985). Jerk is the third time derivative of position; thus, jerk is a measure of smoothness. Flash and her colleagues suggested that curved human movements could be decomposed out of straight movements that minimize jerk (Flash and Henis, 1991). To predict a movement adjustment to a switching target, we add to the original movement a straight movement with minimum-jerk velocity profile. This straight movement starts from the original goal and ends at the new goal position. The overall movement is again curved and ends at the new goal. If the goal does not switch, no change to the original curved movement would occur.

According to the second model, the Vectorial Planning hypothesis, reaching is planned as a hand-centered vector that is adapted by learning a scaling factor and reference axis (Krakauer et al, 2000). In our adaptation (called *Rescale*), we first identify the residual movement starting from the time of goal switch. This movement is curved and ends at the original goal. To make this movement end at the new goal, we rotate and scale the residual movement appropriately. For planar movements, a unique rotation and scaling factor exist. As in the Flash model, the original movement stays unchanged without a goal switch.

For our model, the goodness of fit between the predicted target-switch behavior and the experimental data was significantly better than for the two alternative models. Preliminary results were published beforehand in abstract form (Hoffmann and Schaal, 2007b,a).

## 2 Methods

### 2.1 Subjects

Eight healthy subjects participated (right-handed, 7 males, 1 female, age 23-32 years). They were naive to the purpose of the study. The experiment was approved by the Institutional Review Board of the University of Southern California. Subjects gave informed consent to the experimental protocols prior to their participation.

### 2.2 Apparatus

Subjects were seated in front of a drawing tablet (Wacom, Intuos3,  $9 \times 12$ "), held a stylus pen (Intuos3 grip pen with polyacetal nib), and looked at a computer screen (Dell, 24", wide-screen,  $1920 \times 1200$  pixels) - see Fig. 1A. The distance between eyes and screen was about 60 cm. The drawing area on the tablet ( $9 \times 12$ ") was mapped one-to-one onto the full screen. We updated the screen output at a 60 Hz rate. The experiment was programmed in Matlab (MathWorks), using the Psychophysics Toolbox extensions (Brainard, 1997; Pelli, 1997), version 3.0.8. The software ran under Mac OS X version 10.4.11 on a  $2 \times 3$  GHz Dual-Core Intel Xeon machine.

### 2.3 Experimental protocol

The experiment consists of two blocks, one for each instructed curve, first, spiral, then, oval (Fig. 1B and C). A block had two phases. In the first, subjects practiced tracking a presented curve, which was displayed on the screen. Each curve ended at the center of the screen. Visual feedback was given about the pen's position (gray dot, 6 pixels diameter). In this phase, subjects tracked the curve 20 times. In the second phase, only start and end point of the curve were shown. These points were displayed on the screen as white (start) and green (goal) discs (10 pixels diameter). Subjects were instructed to move the pen quickly from start to goal along a curve resembling the previously trained one. If they moved too slowly, they were instructed to move faster. Subjects were told that they do not need to reproduce exactly the observed curve, instead should move the pen comfortably. Without this instruction, we found in pilot experiments that some subjects tried to reproduce specific geometric features, e.g., vertical alignments, from memory. Subjects were told that the target position may change and that they should end their movement at the new goal (green disc). In half of the trials, chosen randomly, 200 ms after movement onset, the goal

switched to a different position. The new goal position was pseudo-randomly chosen from two alternative locations (150 pixels below the center, or 150 pixels from the center to the right, Fig. 1D). Subjects performed 40 trials to the original goal and 20 trials to each new goal.

Before the actual experiment started, for each block, subjects did a test run with only 10% of the trials in one block. This test run served only to familiarize subjects with the task and setup; we did not record data from this test.

### 2.4 Reaction time experiment

Between first and second block, as a control experiment, we measured the time lag for initiating a new movement for each subject. This experiment was designed to resemble the main experiment while allowing an easily detectable reaction time. Subjects sat in front of the drawing tablet with a pen and looked at the screen. A green disc (10 pixels diameter) was presented at the center of the screen, and subjects were asked to rest with the pen's cursor (gray dot as above) on this disc. With probability 0.5, 400 ms after the pen touched the tablet, the green disc jumped to a different position. This position was either 150 pixel above or below the center (displacements in y-direction, each with probability 0.5). Subjects were asked to move with the pen as quickly as possible to this new position. In total, subjects did 80 reaction-time trials - including trials in which the green disc did not jump. As above, before the actual experiment, subjects did a test run consisting of 4 trials.

### 2.5 Notation

In the following, we introduce the computational model. We write vectors as bold small letters and matrices as bold capital letters. Throughout the paper,  $\mathbf{x}$  is the hand position on the tablet; the position's dependence on time  $t$  is written as  $\mathbf{x}(t)$ . Its time derivative - hand velocity - is  $\dot{\mathbf{x}}$ , and the hand acceleration is  $\ddot{\mathbf{x}}$ .

### 2.6 Mathematical modeling

The dynamics equation for a multi-joint manipulator, like the human arm, can be generally written in joint-angle space  $\boldsymbol{\theta}$  as

$$\mathbf{I}(\boldsymbol{\theta})\ddot{\boldsymbol{\theta}} + \mathbf{c}(\boldsymbol{\theta}, \dot{\boldsymbol{\theta}}) = \boldsymbol{\tau}(\boldsymbol{\theta}, \dot{\boldsymbol{\theta}}, t), \quad (1)$$

where  $\mathbf{I}$  is the inertia matrix,  $\mathbf{c}$  contains the Coriolis and centrifugal forces, and  $\boldsymbol{\tau}$  are the torques produced by a controller including direct and feedback signals (Spong and Vidyasagar, 1989). Here, we ignore gravity since the hand movements are in a plane, and, for simplicity, we ignore friction (Section 3 shows also results for modeling with friction - its effect was small). Apart from friction, the hand is moving freely; thus, no additional external forces are present.

In our model, we are interested in the position of the hand,  $\mathbf{x}(t)$ . Instead of mapping hand position onto joint angles, the dynamics equation can be directly expressed in operational space, i.e., the state variables are hand position,  $\mathbf{x}$ , and velocity,  $\dot{\mathbf{x}}$  (Khatib, 1987),

$$\mathbf{M}(\mathbf{x})\ddot{\mathbf{x}} + \boldsymbol{\mu}(\mathbf{x}, \dot{\mathbf{x}}) = \mathbf{f}(\mathbf{x}, \dot{\mathbf{x}}, t). \quad (2)$$

The variables  $\mathbf{M}$ ,  $\boldsymbol{\mu}$ , and  $\mathbf{f}$  are defined correspondingly to  $\mathbf{I}$ ,  $\mathbf{c}$ , and  $\boldsymbol{\tau}$ . For non-redundant systems, a functional relationship exists between these variables (Khatib, 1987). In our experiment, the arm is close to non-redundant, since the lower arm operates in a plane and subjects did not show noticeable upper body or wrist movements.

To approximate the control function  $\mathbf{f}(\mathbf{x}, \dot{\mathbf{x}}, t)$ , we use the same argument as Shadmehr and Mussa-Ivaldi (1994). The human controller is assumed to incorporate an internal model  $\mathbf{f}_I(\mathbf{x}, \dot{\mathbf{x}}, t)$  of the arm dynamics,

$$\mathbf{f}_I = \hat{\mathbf{M}}(\mathbf{x})\ddot{\mathbf{x}}^*(t) + \hat{\boldsymbol{\mu}}(\mathbf{x}, \dot{\mathbf{x}}). \quad (3)$$

The hatted variables denote estimates of the respective variables, and  $\ddot{\mathbf{x}}^*$  is the desired acceleration. Since the internal model likely deviates from the real dynamics, the solution  $\mathbf{x}(t)$  may diverge from a desired path,  $\mathbf{x}^*(t)$ . To stabilize our controller, we can add a feedback component,

$$\mathbf{f} = \mathbf{f}_I + \mathbf{K}(\mathbf{x}^*(t) - \mathbf{x}) + \mathbf{D}(\dot{\mathbf{x}}^*(t) - \dot{\mathbf{x}}), \quad (4)$$

where the matrices  $\mathbf{K}$  and  $\mathbf{D}$  are the feedback gains (Slotine and Li, 1991). These gains directly relate to the stiffness and viscosity matrices measured at the hand (Shadmehr and Mussa-Ivaldi, 1994; Tsuji et al, 1995). To simplify our resulting dynamic equation, we approximate  $\mathbf{M}(\mathbf{x}) = \text{const}$  and  $\boldsymbol{\mu}(\mathbf{x}, \dot{\mathbf{x}}) = 0$ . We justify these approximations based on a two-link arm simulation, which uses analytic expressions for  $\mathbf{M}(\mathbf{x})$  and  $\boldsymbol{\mu}(\mathbf{x}, \dot{\mathbf{x}})$  (Katayama and Kawato, 1993; Khatib, 1987) and realistic arm parameters (Shadmehr and Mussa-Ivaldi, 1994). One important component in our approximations is the limited range of the hand trajectories. In the simulation, we take typical movements measured during our experiments (Fig. 2).

As result of the simulation, the  $\mathbf{M}$  matrix varied only little: the average normalized standard deviation

(SD) of a matrix entry around its mean value was 7.5% for the spiral shape and 7.7% for oval. Furthermore, the Coriolis and centrifugal term  $\boldsymbol{\mu}$  was small compared to the inertia force  $\mathbf{M}\ddot{\mathbf{x}}$ : the ratio of the average force magnitude between  $\boldsymbol{\mu}$  and  $\mathbf{M}\ddot{\mathbf{x}}$  was 9.6% for spiral and 8.4% for oval.

Given these approximations, our dynamical system is given as

$$\mathbf{M}\ddot{\mathbf{x}} = \hat{\mathbf{M}}\ddot{\mathbf{x}}^*(t) + \mathbf{K}(\mathbf{x}^*(t) - \mathbf{x}) + \mathbf{D}(\dot{\mathbf{x}}^*(t) - \dot{\mathbf{x}}), \quad (5)$$

We combine all time-varying quantities that do not directly depend on state in one function  $\boldsymbol{\xi}(t) = \mathbf{x}^*(t) + \mathbf{K}^{-1}\mathbf{D}\dot{\mathbf{x}}^*(t) + \mathbf{K}^{-1}\hat{\mathbf{M}}\ddot{\mathbf{x}}^*(t)$ , simplifying the dynamics equation to

$$\ddot{\mathbf{x}} = \mathbf{K}_a(\boldsymbol{\xi}(t) - \mathbf{x}) - \mathbf{D}_a\dot{\mathbf{x}}, \quad (6)$$

using  $\mathbf{K}_a = \mathbf{M}^{-1}\mathbf{K}$  and  $\mathbf{D}_a = \mathbf{M}^{-1}\mathbf{D}$ .

This simplified dynamical system is the first step for our final equation of motion. To make the equation converge towards a given goal position  $\mathbf{g}$  and simultaneously add the ability to adjust the motion  $\mathbf{x}(t)$  to a new goal  $\mathbf{g}$ , we assume a controller that transitions towards producing effectively a convergent field around the goal,

$$\ddot{\mathbf{x}}_g = \mathbf{K}_a(\mathbf{g} - \mathbf{x}) - \mathbf{D}_a\dot{\mathbf{x}}; \quad (7)$$

this equation is the same as for a spring-damper system centered at the goal  $\mathbf{g}$ . In behavioral experiments, evidence for a transition between trajectory and endpoint control has been found (Ghez et al, 2007; Scheidt and Ghez, 2007). To realize the transition, we gradually switch from (6) to (7) during the movement, using a time-varying weight  $\gamma(t)$  for (7); thus, our final equation of motion is given as

$$\ddot{\mathbf{x}} = (1 - \gamma)\mathbf{K}_a(\boldsymbol{\xi}(t) - \mathbf{x}) + \gamma\mathbf{K}_a(\mathbf{g} - \mathbf{x}) - \mathbf{D}_a\dot{\mathbf{x}}, \quad (8)$$

where the transition function  $\gamma(t)$  changes from  $\gamma(0) = 0$  to  $\gamma = 1$  at the end of a movement.

For  $\gamma = 1$ , our motion  $\mathbf{x}(t)$  is guaranteed to converge to  $\mathbf{g}$ . We extracted the transition function  $\gamma(t)$  from data (Section 2.7).

To adapt the movement to a new goal, we may change the variable  $\mathbf{g}$  at any time during the movement. Here, we experimentally determined the switch time. In a related robotics study, we showed smooth movement adjustment to new goals if  $\mathbf{g}$  is changed at the beginning of a movement (Hoffmann et al, 2009; Pastor et al, 2009). This model feature agrees with Ghez and Scheidt's interpretation that trajectory and positional control always operate together and not purely react to unexpected target changes (Ghez et al, 2007; Scheidt and Ghez, 2007).

## 2.7 Data analysis

During the experiment, we recorded a subject’s drawing curves (280 in total, including the reaction-time experiment). These curves are given as time series  $\mathbf{x}(t)$  of tablet coordinates at a sampling rate of 60 Hz.

For each curve type, we split the data into the three conditions: original goal, goal-switch position A, and goal-switch position B (Fig. 1D). For the each of these conditions, each subject, and each curve type, a mean curve was computed from the recorded curves.

The recorded raw curves were smoothed with a zero-lag fifth-order Butterworth low-pass filter, with cutoff frequency of 6Hz. First, we describe the computation of the mean curves and, then, the computation of the transition functions (see Section 2.6). Before computing the mean, all curves were scaled and translated in time to correct for variations in speed. For each curve, we determined the time when the tangential velocity first exceeded a threshold (30% of the curve’s maximum tangential velocity) and also the time when the tangential velocity for the first time dropped again below this threshold. Each curve was scaled and translated such that these two time points matched their average values over all curves of the same type and switch condition. Scaling a trajectory changes its sampling rate; thus, we re-sampled each trajectory at 240 Hz by interpolating between sample points (cubic interpolation using function `interp1`, Matlab, MathWorks). A higher sampling rate than the original 60 Hz was chosen to improve accuracy of the integration of the differential equation (Section 2.6). Finally, the mean trajectory was computed as the point-wise average over the pre-processed curves. The resulting mean curve was cut-off at the time when the velocity dropped below 0.01 cm/sec (defining the movement duration  $T$ ).

To compute the transition function  $\gamma(t)$  from data, we compare a trajectory  $\mathbf{x}_1(t)$  towards the original goal  $\mathbf{g}_1$  with a trajectory  $\mathbf{x}_2(t)$  towards a switched goal  $\mathbf{g}_2$ . Based on the difference between the two, we can compute  $\gamma(t)$  even without knowing  $\boldsymbol{\xi}(t)$  by assuming that both  $\gamma(t)$  and  $\boldsymbol{\xi}(t)$  are independent of the goal  $\mathbf{g}$ . Using (8), we obtain for the difference  $\ddot{\mathbf{x}}_1 - \ddot{\mathbf{x}}_2$

$$\ddot{\mathbf{x}}_1 - \ddot{\mathbf{x}}_2 = -\mathbf{K}_a(\mathbf{x}_1 - \mathbf{x}_2) - \mathbf{D}_a(\dot{\mathbf{x}}_1 - \dot{\mathbf{x}}_2) + \gamma\mathbf{K}_a(\mathbf{g}_1 - \mathbf{g}_2). \quad (9)$$

The above equation has to hold for each time point  $t$ , making this equation a matrix equality. Since the equality won’t be exactly fulfilled, due to model uncertainty and noise, we derive  $\gamma(t)$  as the least-squared-error solution of (9),

$$\gamma(t) = \frac{(\mathbf{K}_a\Delta\mathbf{g})^T(\mathbf{K}_a\Delta\mathbf{x}(t) + \mathbf{D}_a\dot{\Delta\mathbf{x}}(t) + \ddot{\Delta\mathbf{x}}(t))}{(\mathbf{K}_a\Delta\mathbf{g})^T(\mathbf{K}_a\Delta\mathbf{g})}, \quad (10)$$

where  $\Delta\mathbf{x} = \mathbf{x}_1 - \mathbf{x}_2$  and  $\Delta\mathbf{g} = \mathbf{g}_1 - \mathbf{g}_2$  (Hastie et al, 2003). We computed  $\gamma(t)$  using the smoothed raw data (see above) for each consecutive trajectory pair consisting of one movement to the original goal and one movement to a different goal. We used consecutive movements instead of mean trajectories to limit the effect of a drifting  $\boldsymbol{\xi}(t)$  during the experiment - subjects may not intend to produce exactly the same movement for each trial. For each curve type and goal (A or B), we averaged  $\gamma(t)$  across all observed trajectory pairs and subjects. To the mean  $\gamma(t)$ , we fitted an exponential function,  $\gamma(t) = 1 - \exp(-(t - t_S)/\tau)$  for  $t \geq t_S$  and  $\gamma(t) = 0$  for  $t < t_S$ , where the switch time  $t_S$  and the relaxation time  $\tau$  were the two parameters determined in the fitting process.

As shown in the Results, the experimentally derived function  $\gamma(t)$  varied between goals and it is apparently sensitive with respect to speed variations along a trajectory. Thus, the assumption preceding Equation (9) is violated, and we will observe an artifact in our estimation of  $\gamma(t)$ . To demonstrate this artifact on  $\gamma(t)$ , we simulated for each subject the target switch according to Equation (8) and using  $\gamma(t) = 1 - \exp(-(t - t_S)/\tau)$ , which does not depend on goal and speed variations. On the predicted trajectory, we manipulated the speed by adding to each time step  $\Delta t$  in the interval  $[0.2s; 0.2s + D]$  the value  $\Delta t(2 \cos(2\pi(t - 0.2s)/D) - 2)$ , where 0.2s is the switch time on screen, and  $D = 1.2s$ . This manipulation has the effect that within this interval, the movement is first slower then faster; while the overall movement duration remains the same. For the resulting trajectory, we computed  $\gamma(t)$  according to Equation (10) and then compared this gamma to the one estimated from data.

## 2.8 Learning of movements

In this section, we explain how we extracted  $\boldsymbol{\xi}(t)$  from data. To compute  $\boldsymbol{\xi}(t)$  for each subject and curve type, we used the average trajectories to the original goal (Section 2.7).

We set  $\mathbf{x}(t)$  to the average trajectory; from this trajectory,  $\dot{\mathbf{x}}(t)$  and  $\ddot{\mathbf{x}}(t)$  are computed through numeric differentiation. Finally, we solve (8) for  $\boldsymbol{\xi}(t)$ ,

$$\boldsymbol{\xi}(t) = \frac{\mathbf{K}_a^{-1}(\ddot{\mathbf{x}}(t) + \mathbf{D}_a\dot{\mathbf{x}}(t)) + \mathbf{x}(t) - \gamma(t)\mathbf{g}}{1 - \gamma(t)}, \quad (11)$$

where  $\mathbf{g}$  is the location of the original goal. These data pairs  $(t, \boldsymbol{\xi})$  can be used by any non-linear supervised learning algorithm to obtain a functional relationship between time and  $\boldsymbol{\xi}$ . Here, we chose linear regression using Gaussian basis functions, as described in (Hoffmann

et al, 2009). We used 25 basis functions, whose parameters were the same as in (Hoffmann et al, 2009). This number of basis functions was sufficient such that our results did not differ between using the learned  $\xi(t)$  or the data pairs  $(\xi, t)$ . Note, since we use linear regression, the solution is analytical and a global optimum (Hastie et al, 2003). After learning  $\xi(t)$ , the generated trajectories from the dynamical system (Equation 8) matched the corresponding experimental mean curves to the original target (spiral: average  $R^2 = 0.9997$ , oval: average  $R^2 = 0.9995$ ).

## 2.9 Choice of model parameters

We took the values of the hand’s stiffness, viscosity, and inertia matrices ( $\mathbf{K}$ ,  $\mathbf{D}$ , and  $\mathbf{M}$ ) from the literature (Tsuji et al, 1995). In Tsuji et al’s experiment, subjects held a robot manipulandum. They were asked to relax their arm and keep it at the fixed position. At the same time, the manipulandum exerted a perturbing force and the resulting forces on the handle were measured; arm and robot were occluded from the subject’s view. Tsuji et al reported the values of the above matrices for each subject and arm posture. We used the values for “hand location 1” and for the setup in which subjects grasped the manipulandum handle instead of being attached to it. These conditions were closest to the conditions in our experiment. We averaged stiffness, viscosity, and inertia matrices across all subjects reported in that work. To keep our mathematical model analytically tractable, we used constant values for  $\mathbf{K}$ ,  $\mathbf{D}$ , and  $\mathbf{M}$ . In humans, however, these matrices depend on posture and velocity of the arm (Gomi and Kawato, 1996; Gribble et al, 1998). We justify our choice given the small range of the movement (Fig. 2). The relevant range is even smaller than the whole movement range: the time-variation of  $\mathbf{K}$ ,  $\mathbf{D}$ , and  $\mathbf{M}$  will affect our resulting movement only in the final movement phase; in the beginning, for  $\gamma(t) \ll 1$ , any variation is compensated by learning an appropriate  $\xi(t)$ , Equation (11). To estimate the effect of inaccuracies in  $\mathbf{K}$  and  $\mathbf{D}$  on our model prediction, we did a sensitivity analysis for these matrices (Section 3.4). In summary, by choosing model parameters from data or literature, we omit tuning a single parameter in our mathematical model to compute the *adjustment* to the switching target.

## 2.10 Alternative models

The predictions of our computational model are compared to two alternatives, which we refer to as “Flash” and “Rescale” model.

### 2.10.1 Flash model

The Flash model is based upon work that suggests that curved human movements are decomposed out of straight movements that minimize a jerk cost (Flash and Hogan, 1985; Flash and Henis, 1991). The jerk cost,  $J$ , is taken as the sum of squared jerk,  $J = \int \|d^3x/dt^3\|^2 dt$ . We refer to a movement that minimizes this jerk cost as a minimum-jerk movement.

Here, we use this concept of composition for adjusting a curved movement to a new target. A movement is adjusted to a new goal by superimposing onto the original movement a minimum-jerk movement between the old and new goal (Flash and Henis, 1991). We added the position vector of this additional movement to the mean trajectory towards the original goal. As starting time of the additional movement, we used the same switch time,  $t_S$ , as for the dynamical-systems model. The minimum-jerk movement ended at the same time as the original movement,  $t = T$ .

### 2.10.2 Rescale model

The Rescale model, assumes a vectorial representation of a movement in extrinsic space in a coordinate frame centered at the hand (Gordon et al, 1994; Krakauer et al, 2000). Movements to different goals are scaled and rotated relative to a vector from hand to goal position. Such planning was consistent with straight movements (Gordon et al, 1994; Krakauer et al, 2000). Here, we adapted this model for curved movements. At the switch time  $t_S$  - same time as for the other models - we scaled and rotated the remaining mean trajectory between the hand position at the current position,  $\mathbf{x}_S$ , and the original goal position,  $\mathbf{g}$ , such that the end-point of the transformed movement overlapped with the new goal,  $\mathbf{g}_N$ . For a movement in two-dimensional space, such a transformation is unique. Let  $\mathbf{x}(t)$  be the nominal movement to the original goal. As new movement  $\mathbf{x}_N(t)$ , we obtain  $\mathbf{x}_N(t) = \alpha \mathbf{R}(\mathbf{x}(t) - \mathbf{x}_S) + \mathbf{x}_S$ , where  $\alpha = \|\mathbf{g}_N - \mathbf{x}_S\| / \|\mathbf{g} - \mathbf{x}_S\|$ , and  $\mathbf{R}$  is the rotational matrix  $[\cos(\phi) \quad -\sin(\phi); \sin(\phi) \quad \cos(\phi)]$  with  $\phi$  being the angle between the vectors  $\mathbf{g} - \mathbf{x}_S$  and  $\mathbf{g}_N - \mathbf{x}_S$  (clockwise rotation from  $\mathbf{g}$  to  $\mathbf{g}_N$ ).

## 2.11 Evaluation of model predictions

The mean curves for the target-switch condition were compared with the model predictions. For each computational model, we computed the coefficient of determination,  $R^2$ , between an experimental mean curve and the corresponding model prediction. In this computation, we used only the part of the trajectory that

followed after we switched the goal  $\mathbf{g}$  in the model, since before this time, there is no difference between models. Explicitly,  $R^2$  was computed as follows. Let  $\mathbf{x}_M(t)$  be the model trajectory and  $\mathbf{x}_E(t)$  the experimental trajectory; then,

$$R^2 = 1 - \frac{\sum_{t=t_S}^T \|\mathbf{x}_M(t) - \mathbf{x}_E(t)\|^2}{\sum_{t=t_S}^T \|\mathbf{x}_E(t) - \bar{\mathbf{x}}_E\|^2}, \quad (12)$$

where  $t_S$  is the time of goal switch in the model and  $\bar{\mathbf{x}}_E$  is the mean of  $\mathbf{x}_E(t)$  in the interval  $[t_S; T]$ . We computed mean values of  $R^2$  by averaging across subjects and the two goal positions, but not across curve types.

To evaluate significant differences of model predictions  $\mathbf{x}_M(t)$  between models, we performed a Wilcoxon test (Wilcoxon, 1945; Siegel, 1956) on the  $R^2$  values between models. This test is an alternative to the paired t-test. The Wilcoxon test, however, does not require Gaussian-distributed measurements. The coefficient of determination is generally non-Gaussian distributed.

### 2.12 Analysis of reaction-time experiment

The reaction times were computed based on the recorded curves  $\mathbf{x}(t)$  from the reaction-time experiment. At the beginning of a trial, subjects hold the pen still; thus,  $\mathbf{x}(t)$  was almost constant. We computed the first time point  $t_J$  when the acceleration (computed in discrete form as  $y(t+2) - 2y(t+1) + y(t)$  in unit “pixels”, with time-step size 1, where  $y$  is the vertical coordinate on screen - along the coronal axis on the tablet) was above a threshold (2 pixels in screen coordinates). As reaction time  $t_R$ , we chose  $t_J$  minus the time when the target disc moved on screen (Section 2.4). For each subject, we computed the average reaction time across trials. We rejected outliers, reaction times that were 5 standard deviations away from the mean, which happened to be the trials in which subjects moved the pen prematurely. Out of a total of 640 trials, only 6 trials were rejected.

## 3 Results

Figure 4 shows the raw trajectories for a sample subject. All subjects could smoothly change their movements to a new target. To draw a curve with the pen, subjects, typically, moved the whole hand (Fig. 3) without moving the fingers; moving the hand matches our assumption in Section 2.6. Only in one subject, we observed a mix of hand and finger movements. The hand movements were carried out speedily: the duration was 1.5 s for the entire curve (Fig. 4).

The following five sections show the experimentally-derived transition function from trajectory to goal-point control, the result of the reaction-time experiment, the accuracy of model predictions for a switching target, the model sensitivity towards changes in the stiffness and viscosity matrices, and the effects of introducing friction in our model.

### 3.1 Transition function

We extracted the transition function  $\gamma(t)$  from the trajectory data (see Section 2.7). The resulting averages for both curve types and goal positions are displayed in Fig. 5A and B. As transition function for our model, we used only a single function  $\gamma(t)$  for all subjects and conditions. In the following, we show how we chose this function and explain the discrepancies of that function to the observation in Fig. 5A.

The transition function that was computed from the data for the oval curve and goal A had the lowest variance and complexity; this function is consistent with a smooth transition towards an attractive field around the goal. The transition resembled an exponential decay (Fig. 5D). A fit to an exponential function (Section 2.7) gave the time  $t_S$  when the transition started (relative to the target switch on screen) and the relaxation time  $\tau$ :  $t_S = 258 \pm 4$  ms and  $\tau = 274 \pm 5$  ms (errors are SE,  $\chi^2 = 0.076$ ,  $n = 99$  data points). We used this exponential transition function for the following prediction of target switching (Section 3.3).

For the spiral curve, however, the transition differed from the exponential function (Fig. 5A). To explain this difference, we did another simulation. On the spiral, three subjects showed a slight decrease in velocity after the target switched. This slow-down may result from subjects getting conservative because the target jump introduces an uncertainty. Thus, we modeled the effect of a momentary slow-down and a subsequent speed-up on the measured transition function (see Methods, Section 2.7). The hereby computed functions resembled the corresponding measured functions for the spiral curve (Figure 5C).

The experimentally obtained transition function also allows a comparison between models. For both Flash and Rescale model, we can predict what the transition function would appear to be if the data were generated according to these models (Fig. 5D). The predictions for both Flash and Rescale were inconsistent with the experimental data.

### 3.2 Reaction time

The time  $t_S$  obtained from the fit of the transition function was close to the result from our reaction time experiment (Fig. 5). The latter gave an average reaction time of  $284 \pm 14$  ms (mean  $\pm$  SE) relative to the target switch on screen (Table 1). Figure 6 shows raw data from this experiment.

Subject (ID)	Reaction time (ms)
1	$247 \pm 30$
2	$258 \pm 29$
3	$287 \pm 33$
4	$299 \pm 36$
5	$258 \pm 28$
6	$374 \pm 53$
7	$279 \pm 43$
8	$269 \pm 35$

**Table 1** Result of reaction-time experiment. Values are mean  $\pm$  SD.

For the further predictions of the target-switching behavior, we used the exponential transition function with parameters  $t_S$  and  $\tau$  as obtained from the fit to the data (see above). First, the mean trajectories to the original goal (Fig. 4) were used to compute the function  $\xi(t)$  for each subject and curve type. Finally, given  $\xi(t)$  and  $\gamma(t)$ , we predict the trajectory change as result of setting the parameter  $\mathbf{g}$  to a new goal position.

### 3.3 Target-switch predictions

The resulting predicted trajectories from our model resembled the experimentally-observed mean curves to the new goals (shown for a sample subject in Fig. 7). This match was observed for both tested curve types and both directions of goal switch and was qualitatively better than for the Flash and Rescale model.

Averaged across all eight participating subjects and both goal-switch directions, the goodness of fit,  $R^2$ , for our model was significantly better than for the two tested alternative models: Flash ( $p = 0.0002$  on spiral and  $p = 0.002$  on oval shape, Wilcoxon test between models,  $n = 16$ ) and Rescale ( $p = 0.04$  on spiral, but  $p = 0.13$  on oval, Wilcoxon test,  $n = 16$ ) - see Fig. 8. For both spiral and oval curves, the average  $R^2$  values for our model were above 0.84; the Flash model showed poor prediction on the oval (average  $R^2 = 0.71$ ), and the Rescale model showed poor prediction on the spiral (average  $R^2 = 0.53$ ).

We observed a difference in the accuracy of our model prediction between the two goal-switch directions (spiral:  $R^2 = 0.93 \pm 0.01$  for goal A and  $R^2 =$

$0.88 \pm 0.03$  for goal B; oval:  $R^2 = 0.91 \pm 0.04$  for goal A and  $R^2 = 0.77 \pm 0.06$  for goal B; values are means  $\pm$  SE,  $n=8$ ). Across all subjects and curve types, this difference was significant ( $p = 0.01$ , Wilcoxon test between goal positions,  $n = 16$ ).

### 3.4 Sensitivity about model parameters

We tested the sensitivity of our model predictions with respect to changes in the stiffness and viscosity matrices,  $\mathbf{K}$  and  $\mathbf{D}$ . Varying  $\mathbf{K}$  by  $\pm 20$  % changed the average  $R^2$  by maximally 3%; varying  $\mathbf{D}$  by  $\pm 20$  % changed the average  $R^2$  by maximally 1 %.

### 3.5 Effect of friction

We tested the effect of friction. For the pen nib, we assume a typical coefficient of friction for polyacetal (Delrin):  $\mu = 0.2^1$ , and for the weight on the pen, we use a typical weight of the lower arm,  $m = 1.52$  kg (Shadmehr and Mussa-Ivaldi, 1994). We re-ran the analysis, adding the dry-friction term  $-m\mu\dot{\mathbf{x}}/|\dot{\mathbf{x}}|$  to Equation (8). For predicting the movement change to a new goal, friction had only a small effect. The coefficient of determination changed by only a small amount, spiral:  $R^2 = 0.90 \pm 0.02$  and oval:  $R^2 = 0.81 \pm 0.07$  (values are means  $\pm$  SE,  $n=16$ ; compare with  $R^2 = 0.91$  and  $R^2 = 0.84$ , Fig. 8).

## 4 Discussion

We studied how humans adjust curved hand movements to a switching target. To our knowledge, this experiment is the first that studies this adjustment for curved movements. The results showed that the change in movement may be explained by a switch of a single control command (goal position), without the need to re-optimize the movement or superimpose optimal paths. Our model predictions were significantly better than for a superposition of minimum-jerk movements (Flash and Henis, 1991) and better than a geometric model that rescales and rotates the remaining part of a desired trajectory. The latter is a realization of the Vectorial Planning hypothesis (Gordon et al, 1994; Krakauer et al, 2000).

Our model used an approximation of limb dynamics. The model assumed a controller that can, first, make the hand go along a curved trajectory and, then, transition towards producing a convergent field for the

<sup>1</sup> [www.plasticsintl.com/datasheets/Delrin\\_150.pdf](http://www.plasticsintl.com/datasheets/Delrin_150.pdf)

hand around the target position. This transition is governed by a continuously changing function, which we extracted from data. The extracted start point of this transition was close to the subjects' reaction time measured in a separate experiment. Here, in all models, the goal position changed instantaneously (close to the measured reaction time). For the Rescale model, this change leads to a discontinuous change in velocity. Thus, this model will improve if adding a mechanism that makes the goal change smoothly from old to new position. To keep the models simple, however, such an addition was omitted in the present analysis.

Each of the alternative models failed on one of the curve types: the Rescale model had a small  $R^2$  on the spiral and the Flash model a small  $R^2$  on the oval curve. The Rescale model is very sensitive to large goal changes relative to the residual distance-to-go. This situation was more prevalent on the spiral curve, where the switch to goal position A was almost twice the distance between hand position at switch time and original goal (Fig. 7). Thus, the Rescale model scaled up inappropriately the remaining part of the movement. The Flash model failed on the oval curve. Here, the measured transition function resembled an exponential decay. The high initial speed of such a decay is in contrast with the gradual acceleration at the beginning of a minimum-jerk movement (Fig. 5D).

In the following two sections, we will discuss the relation of our model to neurophysiology and limits of the model.

#### 4.1 Relation to neurophysiology

Our model and experimental results are closely linked to the current active debate on human motor control. Specifically, they concern the discussions about the combination of equilibrium-point and internal-model control, relevance of convergent force fields, movement representation in the motor cortex, cause of muscle synergies, and use of optimal control.

In the model, we transitioned from trajectory to movement-end-point control. This difference between trajectory and end-point control is supported by visuomotor-adaptation experiments showing a lack of transfer between adaptation to trajectory manipulation and adaptation to end-point manipulation (Ghez et al, 2007; Scheidt and Ghez, 2007).

At the beginning of a movement, an internal model may be used to keep the hand along a desired path, as has been discussed in many works, e.g., (Shadmehr and Mussa-Ivaldi, 1994; Gomi and Kawato, 1996; Popescu and Rymer, 2000; Hinder and Milner, 2003). At the

end of a movement, the goal (or target) acts as an equilibrium point, a feature that is shared with the equilibrium-point hypothesis (Feldman, 1986). The corresponding convergent force field<sup>2</sup> may arise from the following sources:

1. The muscle-tendon apparatus has spring-like characteristics (Zajac et al, 1989).
2. Muscle spindles provide feedback of muscle extension. The corresponding feedback loop on the spinal-cord level may act to drive the muscle back to a desired state (Loeb et al, 1999).
3. The shape of the force field depends on the biomechanical properties of the arm, e.g., its geometry (Shadmehr and Wise, 2005).

Generally, this force field will be non-linear. In our model, we used a linear term. This term can be interpreted as a first-order approximation, computed through Taylor expansion of the non-linear field.

The role of the visual feedback is to set the position of the force field (goal variable  $\mathbf{g}$ ). To obtain this position, the brain has to transform the target from eye-centered coordinates into arm posture: such transformations have been actively researched in neurophysiology (Snyder, 2000).

Convergent force fields have been also discussed in the context of frog-leg force and movement control (Bizzi et al, 1991; Giszter et al, 1993; Mussa-Ivaldi and Bizzi, 2000). This work has greatly influenced our concept of modularity in control. A force field can be observed at the foot as a result of micro-stimulating the spinal cord at specific locations. If stimulating simultaneously two locations, a new field can be observed that resembles the linear combination of the two fields that would result from stimulating each single site individually. Thus, the individual fields could form building blocks for more complex dynamics. Interestingly, we also combine linearly two fields: a trajectory generating field (Equation 6) and a convergent field around the target (Equation 7). How far the insights from frog-leg force fields extend to the human is still an open question though.

Being able to explain movement adjustment with a single parameter implies a reduction in control parameters compared to the complexity of a movement. This observation is in agreement with recent findings on M1 motor neurons. Recent experiments indicate that single neurons encode complex movement fragments (Hatsopoulos et al, 2007), which reflect the spatiotemporal complexity of the musculoskeletal system (Pruszynski et al, 2010). In agreement with this work, our model

<sup>2</sup> In our model, we used an acceleration field, but these two field types are closely linked through the multiplication of an inertia term.

links the movement representation directly to the arm dynamics, instead of using a higher-level abstraction, as originally assumed for a next-state planner (Shadmehr and Wise, 2005). In addition, related to our work, a recent computational model showed that the computation by spinal cord and spindle feedback loops may account for many low-level movement phenomena, like, e.g., perturbation rejection (Raphael et al, 2010). Thus, the top down commands may be fairly simple.

If the number of control parameters is small compared to the number of muscles involved, correlations between muscles will be observed. For human movement, such correlation has been indeed found and termed “synergies” (d’Avella et al, 2003; Hart and Giszter, 2004; Ting and Macpherson, 2005; Bizzi et al, 2008). The level at which synergies are formed is still debated. For example, a recent study suggested flexible grouping of muscles during force production (Kutch et al, 2008).

Different from our dynamical model, a popular hypothesis for human motor control suggests movement generation between two targets as result of an off-line optimization process (Flash and Hogan, 1985; Stein et al, 1986; Kawato, 1996; Harris and Wolpert, 1998; Todorov and Jordan, 1998). Unclear, however, remains how such optimization results in movements that are flexible to adjust to changes in the environment, like changing movement targets. Recomputing the optimization to adjust for a new target appears computationally too expensive to account for the fast adjustments found in human movements.

An alternative to the above cited optimization methods is optimal feedback control (OFC) (Maybeck, 1979; Todorov and Jordan, 2002), which computes a series of feedback gains. Thus, OFC could cope with a changing target, if this target appears in the feedback error. However, OFC by itself cannot explain the generation of curved trajectories, as studied in the present work. A fundamental difference between OFC and the present model is that the latter includes a kinematic representation of a curved movement. Our experiment does indeed show that subjects reproduce curve movements from instruction, suggesting a kinematic representation. In contrast, OFC as a model for human movements tries to explain their generation without any kinematic representation (Todorov and Jordan, 2002; Liu and Todorov, 2007).

#### 4.2 Limits on our model

Our model predictions matched the behavioral data better than the two alternative tested models. However, this article does not mean to imply that the simple model in Equation (8) is a principal or accurate

model of human function; rather, the equation should be viewed as an approximation of a more complex dynamical system, which however shares the same features as our model, namely the transition towards a convergent field around the goal, and just by moving this field, the whole trajectory can be automatically adjusted.

We justified our approximations with a simulation of the non-linear dynamics: variations of around 7-10 % were ignored. Moreover, inaccuracies in model parameters (stiffness and viscosity) as well as friction had only a small effect on our model prediction. The ignored variations in dynamics, however, could be responsible for the small mismatch between model prediction and experimental data (Fig. 7).

Part of our model is a function that regulates the transition of the dynamics towards a field converging at the goal. The estimation of this transition function from data is sensitive to trial-by-trial variations of a movement (see Section 2.7). Thus, our estimation contains artifacts (here, presumably, deviations from an exponential function). For the spiral movement, we could show that speed variations may explain these artifacts.

For the transition function, we can further explain the difference in artifact between the two goal positions A and B. At the time of goal switch, the hand moves approximately orthogonal to the goal change towards position A. Thus, the speed changes are also orthogonal to the goal change. According to Equation (10), these changes are projected onto the goal change direction. Therefore, they largely vanish and have a minor effect on the estimation of  $\gamma$  from data. In contrast, for goal position B, the velocity changes are in the same direction as the goal change, and the projection does not cancel those changes. Consistent with this analysis, for both oval and spiral movements, the deviations from the exponential transition function were larger for goal position B (Fig. 5). In addition, the predicted trajectories fitted the experimental data better for goal A than for goal B (Results, Target-switch predictions), again consistent with the above argument.

A further limitation of our dynamics approximation is the distance of goal change. We showed movement adjustments for only a small change in goal position (about 3 cm). Indeed for larger changes (about 10 cm), pilot experiments showed larger deviations between model prediction and human movement. Possibly, larger changes require a different recruitment of control commands in humans. Moreover, our model approximation will become more inaccurate with increasing range of motion.

As a future step, it would be interesting to simulate a more detailed musculoskeletal model, e.g., using Rah-

man Davoodi's Musculoskeletal Modeling in Simulink software (Biomedical Engineering, University of Southern California). A possible compound of such a step is that the gained precision might be irrelevant given the large variability of human motion - for a single subject as well as between subjects.

## 5 Conclusion

In our experiment, humans smoothly adjusted curved movements to new targets. The resulting motion was inconsistent with two models for this adjustment: (1) superimposing a new minimum-jerk movement on top of the original movement and (2) rescaling and rotating the movement to end at the new goal.

As possible alternative, we showed that movements could be generated with a dynamical system based on limb and controller dynamics, and movements could be adjusted to a new target just by changing a goal parameter in the model. These results suggest trajectory generation using only a few control parameters.

We already applied the insight from this experiment about how to adjust a trajectory with a single goal parameter to the control of a robotic arm (Hoffmann et al, 2009). There, we could make the robot reproduce a demonstrated trajectory, like placing a cup on a table, and then generalize this trajectory to new target positions, again, just by changing the goal variable. Such a mechanism could benefit the control of prosthetic limbs and electrically-stimulated paralyzed limbs. A challenge of prosthetic control, e.g. is the limited number of control parameters that can be extracted from the patient - a challenge that we addressed with this work.

**Acknowledgements** I am grateful to Drs Stefan Schaal, Simon Giszter, and Francisco Valero-Cuevas for helpful discussions, particularly, about the interpretation and presentation of the results. Furthermore, I like to thank Dr John Krakauer for suggesting to extract the transition function from data and Dr Scott Young and the anonymous reviewers for their comments which helped to improve the manuscript. The experiments were performed in the Computational Learning & Motor Control Lab of Dr Schaal. This work was supported by grant HO-3771-1 from the German Research Foundation (DFG).

## References

Alexander RM (1995) Simple models of human motion. *Appl Mech Rev* 48:461–469  
 Bizzi E, Mussa-Ivaldi FA, Giszter SF (1991) Computations underlying the execution of movement: A biological perspective. *Science* 253(5017):287–291

Bizzi E, Cheung V, d'Avella A, Saltiel P, Tresch M (2008) Combining modules for movement. *Brain Research Reviews* 57(1):125–133  
 Brainard DH (1997) The psychophysics toolbox. *Spatial Vision* 10:433–436  
 Bullock D, Grossberg S (1988) Neural dynamics of planned arm movements: Emergent invariants and speed-accuracy properties during trajectory formation. *Psychological Review* 95(1):49–90  
 d'Avella A, Saltiel P, Bizzi E (2003) Combinations of muscle synergies in the construction of a natural motor behavior. *Nature Neuroscience* 6(3):300–308  
 Feldman AG (1986) Once more on the equilibrium-point hypothesis (lambda model) for motor control. *Journal of Motor Behavior* 18(1):17–54  
 Flash T, Henis E (1991) Arm trajectory modifications during reaching towards visual targets. *Journal of Cognitive Neuroscience* 3(3):220–230  
 Flash T, Hogan N (1985) The coordination of arm movements: an experimentally confirmed mathematical model. *J Neurosci* 5(7):1688–1703  
 Ghez C, Scheidt R, Heijink H (2007) Different Learned Coordinate Frames for Planning Trajectories and Final Positions in Reaching. *Journal of Neurophysiology* 98(6):3614–3626  
 Giszter SF, Mussa-Ivaldi FA, Bizzi E (1993) Convergent force fields organized in the frog's spinal cord. *Journal of Neuroscience* 13(2):467–491  
 Gomi H, Kawato M (1996) Equilibrium-Point Control Hypothesis Examined by Measured Arm Stiffness During Multijoint Movement. *Science* 272(5258):117–120  
 Gordon J, Ghilardi MF, Ghez C (1994) Accuracy of planar reaching movements. *Experimental Brain Research* 99(1):97–111  
 Gribble PL, Ostry DJ, Sanguineti V, Laboissiere R (1998) Are Complex Control Signals Required for Human Arm Movement? *J Neurophysiol* 79(3):1409–1424  
 Harris CM, Wolpert DM (1998) Signal-dependent noise determines motor planning. *Nature* 394(6695):780–784  
 Hart CB, Giszter SF (2004) Modular Premotor Drives and Unit Bursts as Primitives for Frog Motor Behaviors. *J Neurosci* 24(22):5269–5282  
 Hastie T, Tibshirani R, Friedman JH (2003) *The Elements of Statistical Learning*. Springer  
 Hatsopoulos N, Xu Q, Amit Y (2007) Encoding of movement fragments in the motor cortex. *J Neurosci* 27:5105–5114  
 Hinder MR, Milner TE (2003) The case for an internal dynamics model versus equilibrium point control in human movement. *J Physiol* 549:953–963

- Hoff B, Arbib MA (1993) Models of trajectory formation and temporal interaction of reach and grasp. *Journal of Motor Behavior* 25(3):175–192
- Hoffmann H, Schaal S (2007a) A computational model of human trajectory planning based on convergent flow fields. In: Society for Neuroscience, Abstracts, San Diego, CA
- Hoffmann H, Schaal S (2007b) Human movement generation based on convergent flow fields: a computational model and a behavioral experiment. In: Shadmehr R, Todorov E (eds) *Advances in Computational Motor Control VI*, San Diego, CA
- Hoffmann H, Pastor P, Park DH, Schaal S (2009) Biologically-inspired dynamical systems for movement generation: Automatic real-time goal adaptation and obstacle avoidance. In: *IEEE International Conference on Robotics and Automation*, Kobe, Japan
- Ijspeert AJ, Nakanishi J, Schaal S (2002) Movement imitation with nonlinear dynamical systems in humanoid robots. In: *International Conference on Robotics and Automation*, IEEE, Washington, DC, pp 1398–1403
- Ijspeert AJ, Nakanishi J, Schaal S (2003) Learning attractor landscapes for learning motor primitives. In: Becker S, Thrun S, Obermayer K (eds) *Advances in Neural Information Processing Systems*, MIT Press, Cambridge, MA, vol 15, pp 1523–1530
- Katayama M, Kawato M (1993) Virtual trajectory and stiffness ellipse during multijoint arm movement predicted by neural inverse models. *Biological Cybernetics* 69:353–362
- Kawato M (1996) Bi-directional theory approach to integration. In: Konczak J, Thelen E (eds) *Attention and Performance XVI*, MIT Press, Cambridge, MA, pp 335–367
- Khatib O (1987) A unified approach for motion and force control of robot manipulators: The operational space formulation. *IEEE Journal of Robotics and Automation* RA-3(1):43–53
- Krakauer JW, Pine ZM, Ghilardi MF, Ghez C (2000) Learning of Visuomotor Transformations for Vectorial Planning of Reaching Trajectories. *J Neurosci* 20(23):8916–8924
- Kutch JJ, Kuo AD, Bloch AM, Rymer WZ (2008) End-point force fluctuations reveal flexible rather than synergistic patterns of muscle cooperation. *J Neurophysiol* 100(5):2455–71
- Liu D, Todorov E (2007) Evidence for the Flexible Sensorimotor Strategies Predicted by Optimal Feedback Control. *Journal of Neuroscience* 27(35):9354–9368
- Loeb GE, Brown IE, Cheng EJ (1999) A hierarchical foundation for models of sensorimotor control. *Experimental Brain Research* 126(1):1–18
- Maybeck P (1979) *Stochastic Models Estimation and Controls*. Prentice Hall
- Mussa-Ivaldi FA, Bizzi E (2000) Motor learning through the combination of primitives. *Philosophical Transactions of the Royal Society of London Series B* 355:1755–1769
- Pastor P, Hoffmann H, Asfour T, Schaal S (2009) Learning and generalization of motor skills by learning from demonstration. In: *IEEE International Conference on Robotics and Automation*, Kobe, Japan
- Pelli DG (1997) The videotoolbox software for visual psychophysics: Transforming numbers into movies. *Spatial Vision* 10:437–442
- Popescu FC, Rymer WZ (2000) End Points of Planar Reaching Movements Are Disrupted by Small Force Pulses: An Evaluation of the Hypothesis of Equifinality. *Journal of Neurophysiology* 84(5):2670–2679
- Pruszynski JA, Lillicrap TP, Scott SH (2010) Complex Spatiotemporal Tuning in Human Upper-Limb Muscles. *Journal of Neurophysiology* 103:564–572
- Raphael G, Tsianos GA, Loeb GE (2010) Spinal-Like Regulator Facilitates Control of a Two-Degree-of-Freedom Wrist. *J Neurosci* 30(28):9431–9444
- Scheidt RA, Ghez C (2007) Separate Adaptive Mechanisms for Controlling Trajectory and Final Position in Reaching. *Journal of Neurophysiology* 98(6):3600–3613
- Shadmehr R, Mussa-Ivaldi F (1994) Adaptive representation of dynamics during learning of a motor task. *J Neurosci* 14(5):3208–3224
- Shadmehr R, Wise SP (2005) *The Computational Neurobiology of Reaching and Pointing*. MIT Press
- Siegel S (1956) *Non-parametric statistics for the behavioral sciences*. McGraw-Hill, New York
- Slotine J, Li W (1991) *Applied nonlinear control*. Prentice Hall, Englewood Cliffs, NJ
- Snyder LH (2000) Coordinate transformations for eye and arm movements in the brain. *Current Opinion in Neurobiology* 10:747–754
- Spong MW, Vidyasagar M (1989) *Robot Dynamics and Control*. Wiley
- Stein RB, Oguztoreli MN, Capaday C (1986) What is optimized in muscular movements? In: Jones NL, McCartney N, McComas AJ (eds) *Human Muscle Power*, Human Kinetics Publisher, Champaign, Illinois, pp 131–150
- Ting LH, Macpherson JM (2005) A Limited Set of Muscle Synergies for Force Control During a Postural Task. *J Neurophysiol* 93(1):609–613
- Todorov E, Jordan MI (1998) Smoothness Maximization Along a Predefined Path Accurately Predicts the Speed Profiles of Complex Arm Movements. *J Neu-*

- 
- rophysiol 80(2):696–714
- Todorov E, Jordan MI (2002) Optimal feedback control as a theory of motor coordination. *Nature Neuroscience* 5(11):1226–1235
- Tsuji T, Morasso PG, Goto K, Ito K (1995) Human hand impedance characteristics during maintained posture. *Biological Cybernetics* 72(6):475–485
- Viviani P, Flash T (1995) Minimum-jerk, two-thirds power law, and isochrony: Converging approaches to movement planning. *Journal of Experimental Psychology: Human Perception and Performance* 21(1):32–53
- Wilcoxon F (1945) Individual comparisons by ranking methods. *Biometrics* 1:80–83
- Zajac FE, Biosci J, *Physiol JC*, *Biol JE*, *Physiol ZV*, *Lond JZ*, *Physiol ZJ*, *Soc JGE*, *Acta BB*, *Biochem A* (1989) Muscle and tendon: properties, models, scaling, and application to biomechanics and motor control. *Crit Rev Biomed Eng* 17:359–411

**Fig. 1** Experimental setup. A: Subjects sit at a graphics tablet and look at a screen. B: Screen display of spiral curve for the tracking phase shown with start point (circle) and end point (disc). C: Display of oval curve. D: Locations on screen of the original goal (black disc) and the new goal positions (diamonds).

**Fig. 2** Simulated two-link arm shown in typical initial posture together with typical curve movements (red): (A) spiral and (B) oval. Link lengths and curves are true to scale.

**Fig. 3** Movie sequence for typical spiral (A) and oval (B) movements. For clarification, start and goal position are shown overlaid as white and green discs. The images are a top-down view of the digitizing tablet.

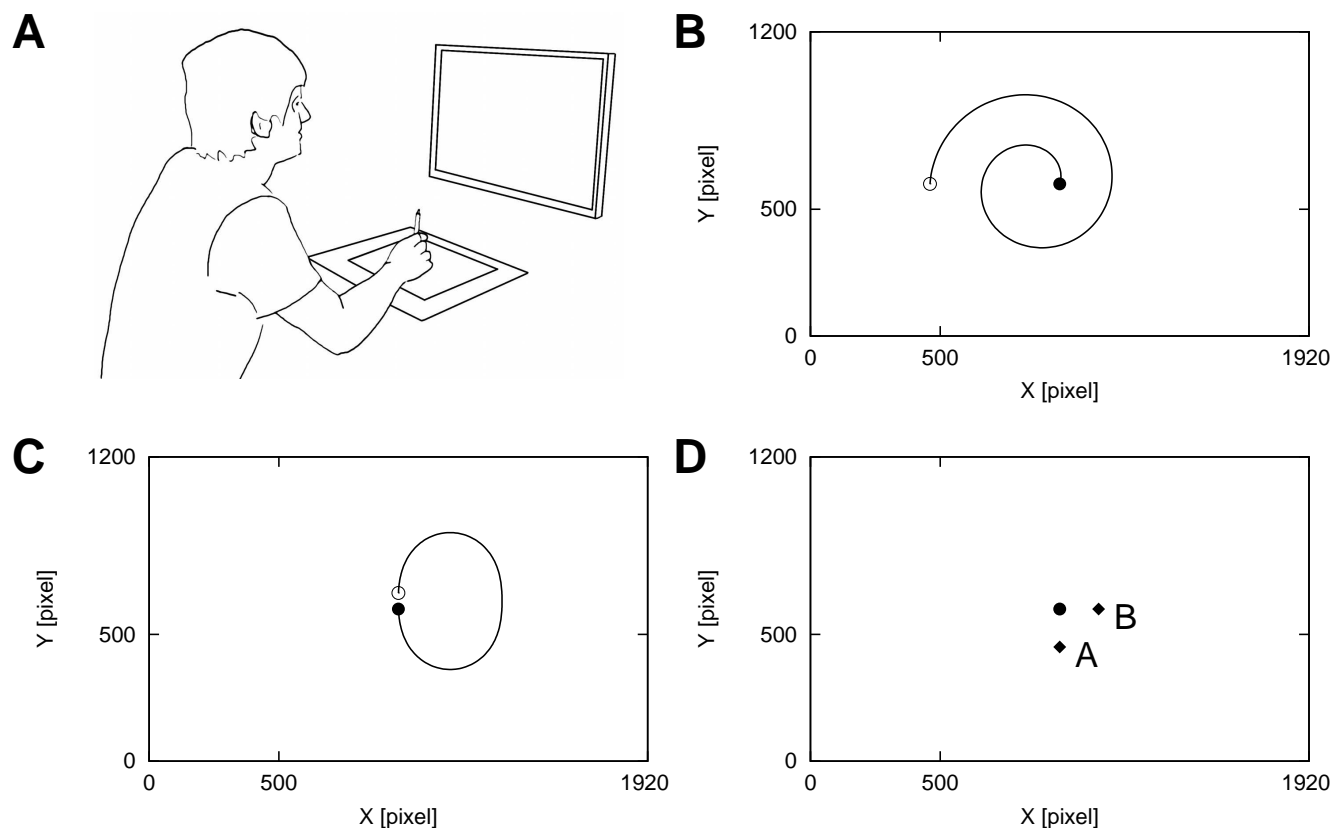
**Fig. 4** Results of goal-switching experiment, shown for subject 2. On the left of each block are the pen-position traces on the tablet: recorded raw curves are shown in light colors (yellow for original goal and cyan for goal switch); dark colors are for mean trajectories (red for original goal and dashed blue for goal switch). On the right are the tangential velocity profiles corresponding to the mean trajectories on the left. The time of goal-switch is marked by a dashed vertical line. A, B, C, and D show different curves and target-switch positions.

**Fig. 5** Transition functions,  $\gamma(t)$ , extracted from data for each curve type, spiral (A) and oval (B), and goal position. Curves show mean  $\pm$  SE. (C) Simulated transition functions assuming speed variations (see text) for the spiral curve and both goal positions. (D) Transition function for the oval curve, goal A, compared to model predictions. For our model (DYN), the curve is a fit to the data. Curves show mean  $\pm$  SE. The transition function for the Flash model can be computed analytically and, thus, does not show errors. For comparison, the result from the reaction-time experiment is shown (arrow).

**Fig. 6** Result of reaction-time experiment, shown for subject 5. A: Raw curves (gray) recorded from subject. All 40 trials with switching target are shown. The time of goal-switch on screen was set to 0. The arrow points at the computed mean value (258 ms) for this subject. B: Histogram of reaction times as obtained from single trials.

**Fig. 7** Comparison of model predictions with experiment. From the experiment, the average curves to the original goal (red) and to the new goal (blue) are shown. Our dynamical-systems model, DYN (green) is compared to the Flash model (gray) and Rescale model (black). Panels A and B show the results for the spiral movements and panel C and D for the oval movements (one panel each for each new goal position).

**Fig. 8** Goodness of fit for target-switch prediction (A for spiral and B for oval curve).  $R^2$  values are compared between predictions for all three tested models. DYN refers to our dynamical-system model. Bars show means  $\pm$  SE,  $n = 16$ .



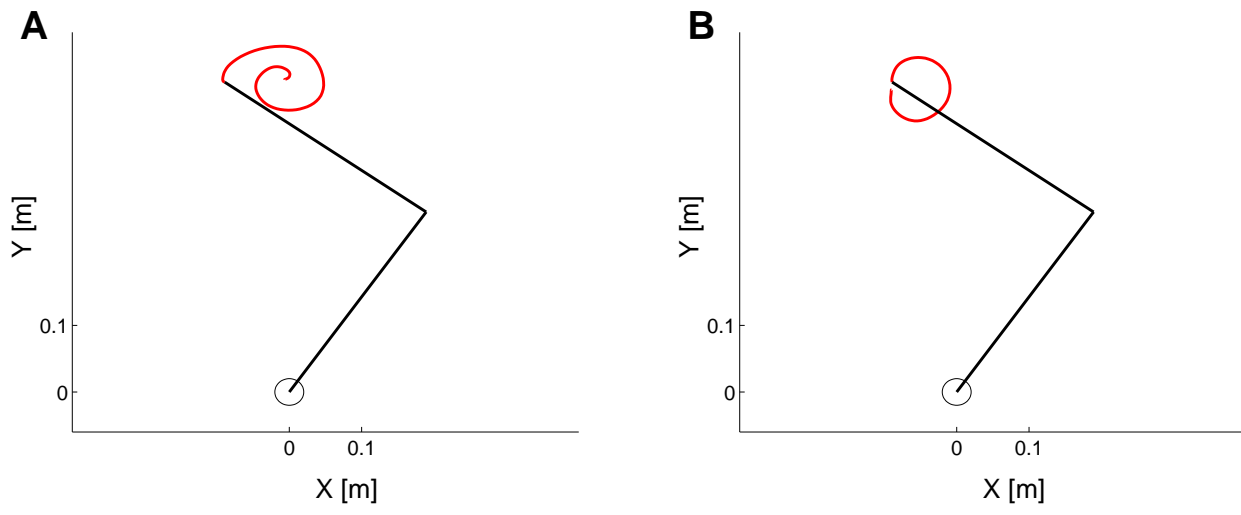


Figure 2

**A****B**

Figure 3

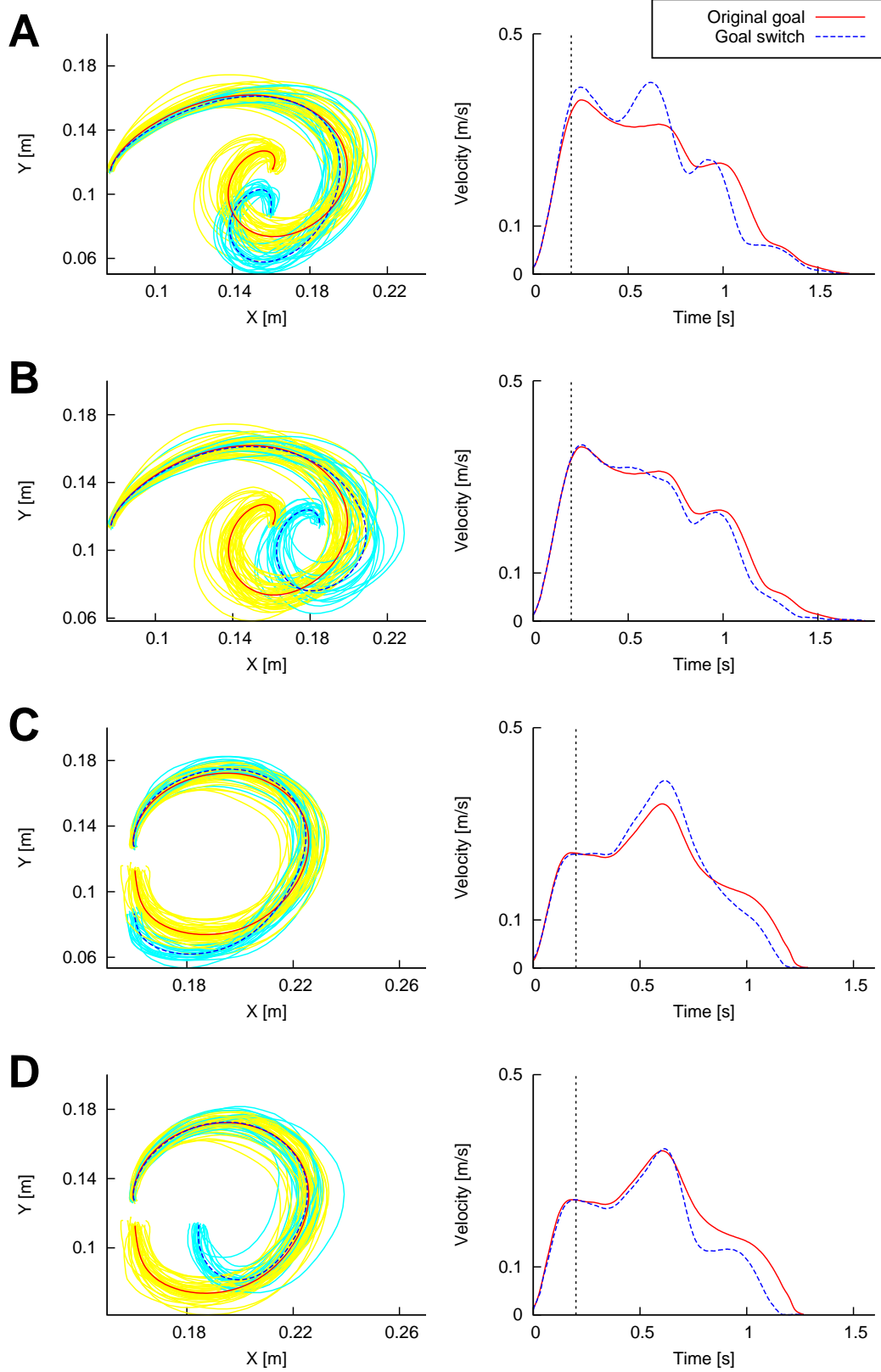


Figure 4

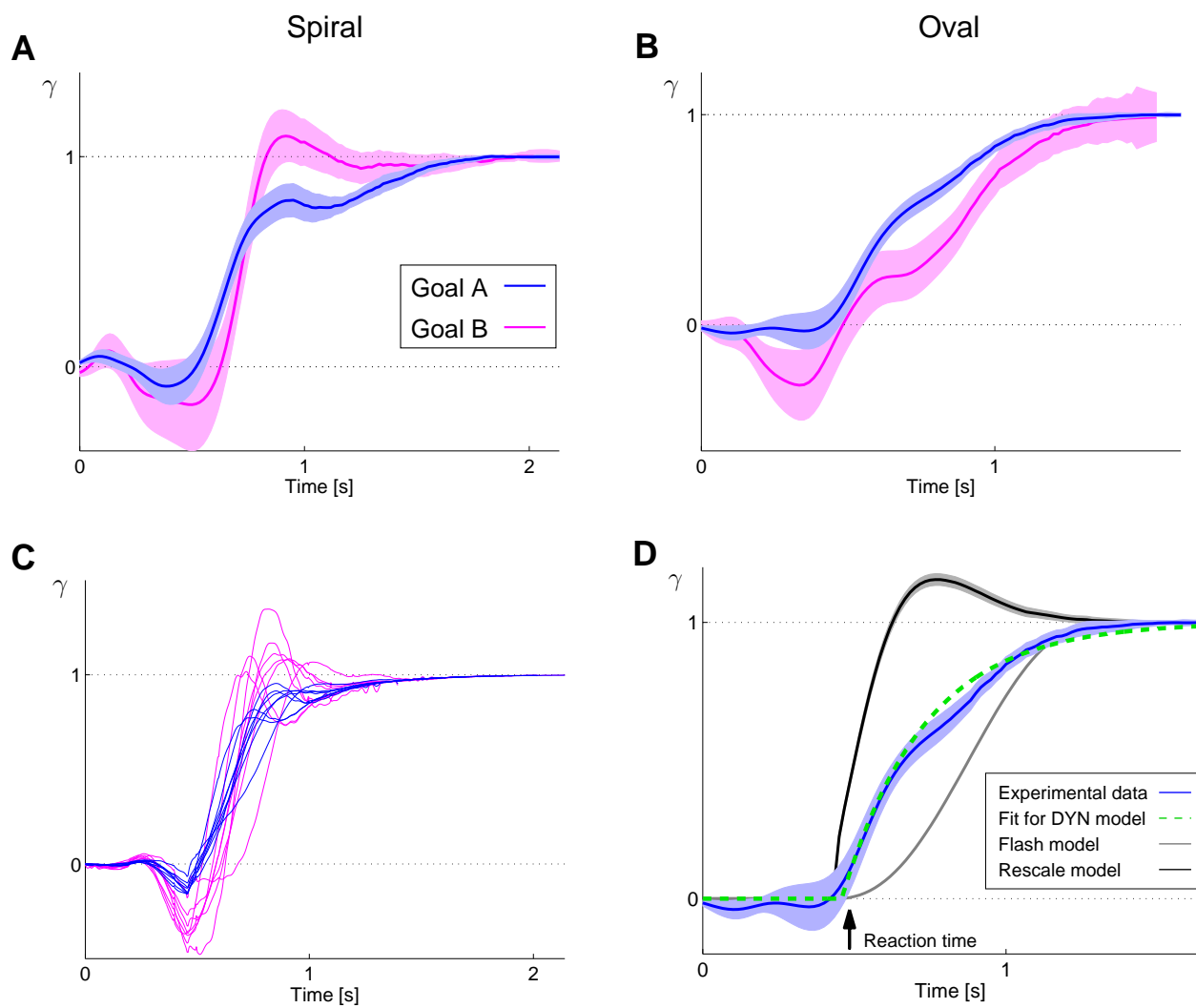


Figure 5

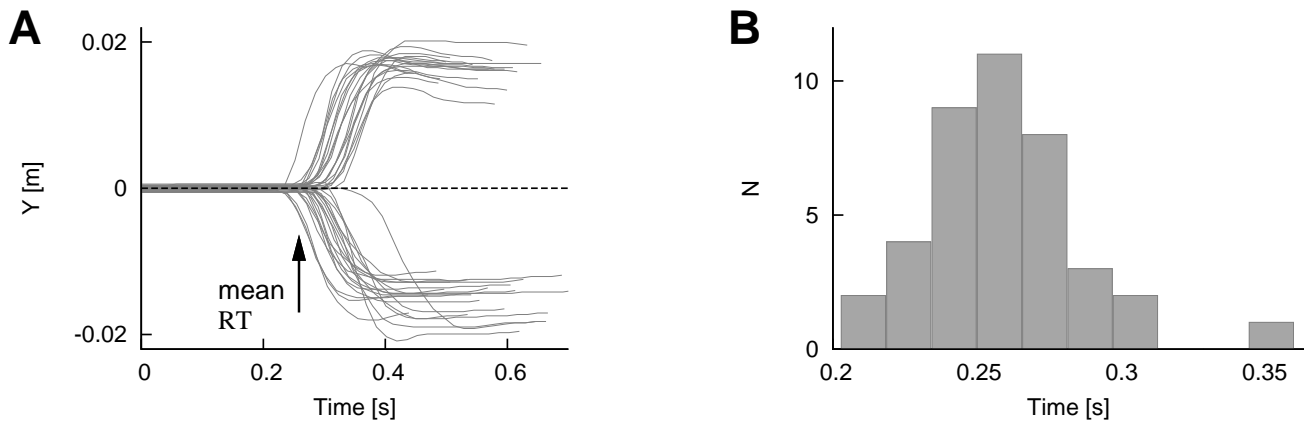


Figure 6

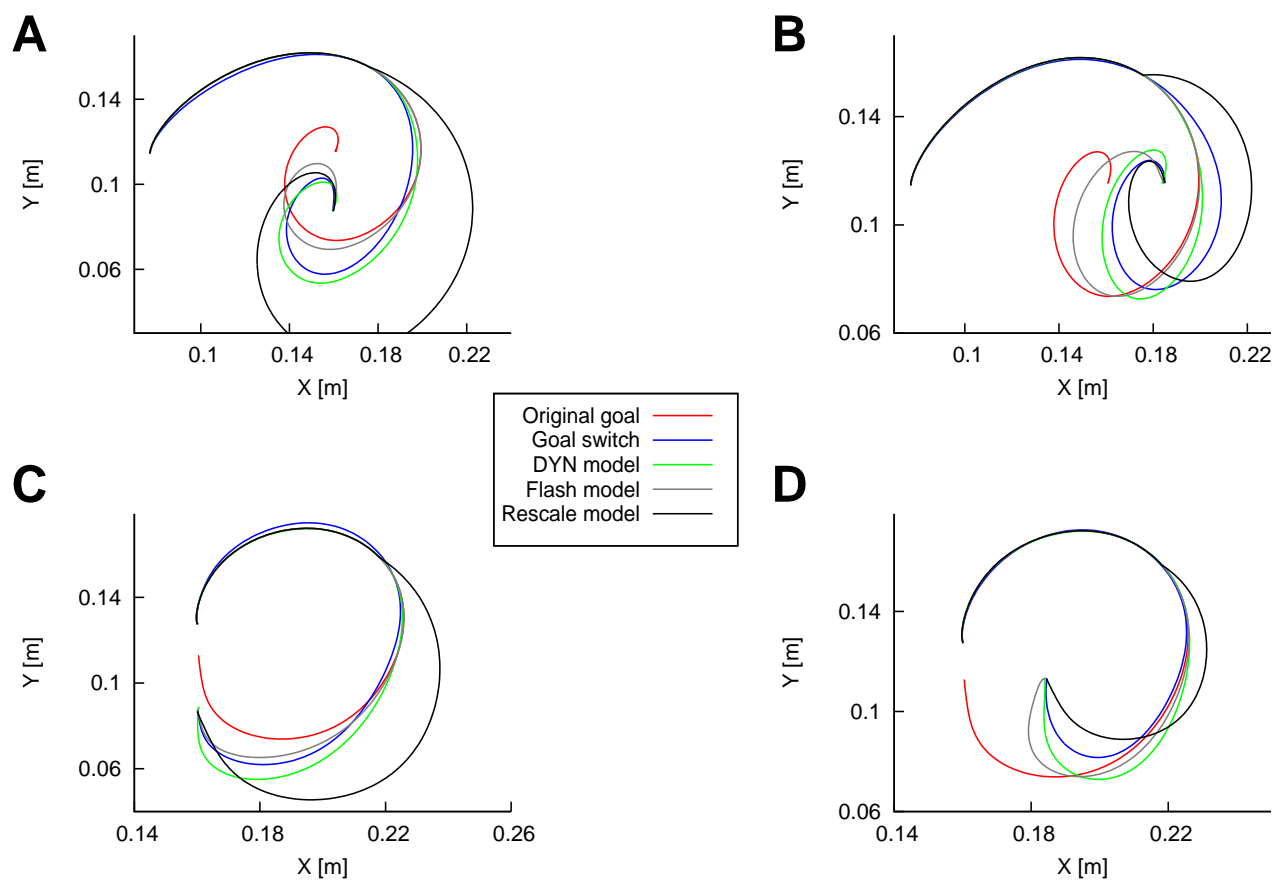


Figure 7

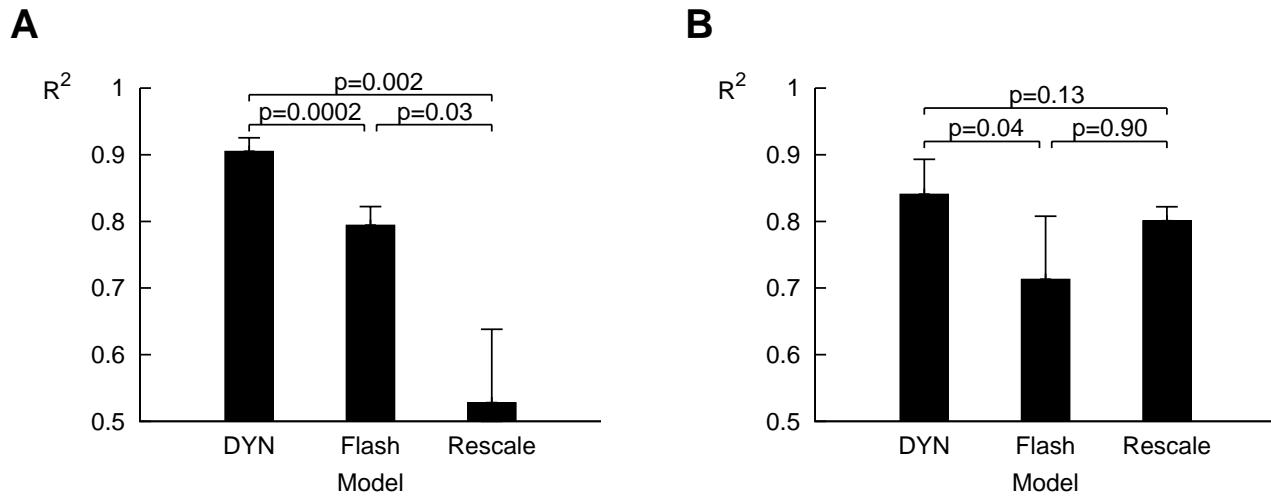


Figure 8